The EMBO Journal Vol.18 No.13 pp.3558–3563, 1999

Projection structure of NhaA, a secondary transporter from *Escherichia coli*, at 4.0 Å resolution

Karen A.Williams[1], Ulrike Geldmacher-Kaufer, Etana Padan[2], Shimon Schuldiner[2] and Werner Kühlbrandt

Max-Planck-Institute of Biophysics, Department of Structural Biology, Heinrich-Hoffmann-Strasse 7, D-60528 Frankfurt am Main, Germany and [2]The Hebrew University of Jerusalem, Department of Microbial and Molecular Ecology, The Institute of Life Sciences, 91904 Jerusalem, Israel

[1]Corresponding author
e-mail: williams@biophys.mpg.de

Electron cryomicroscopy of frozen-hydrated two-dimensional crystals of NhaA, a Na^+/H^+ antiporter from *Escherichia coli* predicted to have 12 transmembrane α-helices, has facilitated the calculation of a projection map of NhaA at 4.0 Å resolution. NhaA was homologously expressed in *E.coli* with a His_6 tag, solubilized in dodecyl maltoside and purified in a single step using Ni^{2+} affinity chromatography. Two-dimensional crystals were obtained after reconstitution of purified protein with *E.coli* lipids. The projection map reveals that this secondary transporter has a highly asymmetric structure in projection. NhaA exhibits overall dimensions of ~38 × 48 Å with a ring-shaped density feature probably corresponding to a bundle of tilted helices, adjacent to an elongated region of density containing several peaks indicative of transmembrane helices. Two crystal forms with $p22_12_1$ symmetry show tightly packed dimers of NhaA which differ in the interactions between adjacent dimers. This work provides the first direct glimpse into the structure of a secondary transporter.

Keywords: electron cryomicroscopy/*Escherichia coli*/ Na^+/H^+ antiporter/two-dimensional crystallization

Introduction

NhaA, a 42 kDa Na^+/H^+ antiporter from *Escherichia coli* inner membranes, is the focus of the present investigation into the structure of a secondary transporter using electron crystallography. Secondary transporters comprise a large and diverse group, and mediate the movement of small substrates including ions, sugars and amino acids across cell membranes using energy supplied by transmembrane ion gradients. In order to fully understand how these proteins couple substrate transport to the proton or sodium motive force, detailed structural information is required. At present, however, very little direct structural information is available for any secondary transporter. *Escherichia coli* transporters provide excellent systems for structural studies because of the relative ease of overexpression and purification of these proteins. Analysis of the *E.coli* genome demonstrates the presence of ~160 secondary transporters in 65 families ranging from 110–500 amino acids in length, with the most common topology predicted to be that of 12 transmembrane (TM) helices (Paulsen *et al*., 1998).

NhaA, one of three Na^+/H^+ antiporters in *E.coli*, is a member of the prokaryotic NhaA family which functions principally in the adaptation to high salinity and alkaline pH (for reviews see Padan and Schuldiner, 1994a,b, 1996). NhaA uses the driving H^+ gradient to expel Na^+ from the cell, thereby preventing Na^+ toxicity as well as helping to maintain the Na^+ gradient used by other secondary transporters. This 388 residue protein is predicted to have 12 TM α-helices, with the 7th and 8th TM helices appearing shorter than usual (Rothman *et al*., 1996). NhaA exhibits a stoichiometry of 2 H^+:1 Na^+ and its activity is markedly influenced by pH (Taglicht *et al*., 1991). Activity increases by ~1000-fold between pH 7 and 8, and is correlated with a conformational change (Rothman *et al*., 1997). NhaA is homologously overexpressed in *E.coli* with a His_6 tag, and can be obtained in milligram quantities after solubilization of membranes in dodecyl maltoside and purification on a single Ni^{2+} chelation chromatography column (Olami *et al*., 1997).

Electron crystallography has emerged as a powerful tool to determine the structure of membrane proteins from two-dimensional (2D) crystals (Walz and Grigorieff, 1998), including several of them close to atomic resolution (Henderson *et al*., 1990; Kühlbrandt *et al*., 1994; Kimura *et al*., 1997). 2D crystals of a number of secondary transporters have been obtained previously, including the membrane domain of human erythrocyte Band 3 (Wang *et al*., 1993, 1994), full-length Band 3 (Dolder *et al*., 1993), homologously overexpressed *E.coli* melibiose permease (Rigaud *et al*., 1997) and lactose permease (Zhuang *et al*., 1999). All of these studies were conducted in negative stain and as a result provide low resolution insights into the overall size and shape of these transport proteins. The 2D crystallization of NhaA was undertaken in an effort to obtain large, well ordered crystals so that electron cryomicroscopy could be used to uncover internal structural details of this representative secondary transport protein.

Results and discussion

Two-dimensional crystallization trials of NhaA have yielded a variety of crystal forms with different crystal morphologies, lattices and symmetries, and exhibiting varying degrees of order and stability (K.A.Williams, manuscript in preparation). Well ordered NhaA 2D crystals were obtained after detergent removal by dialysis and take the form of tubular vesicles which are 0.4–1.0 μm in width and 0.7–4.0 or more micrometers in length (Figure 1). These crystals flatten on the microscope grid

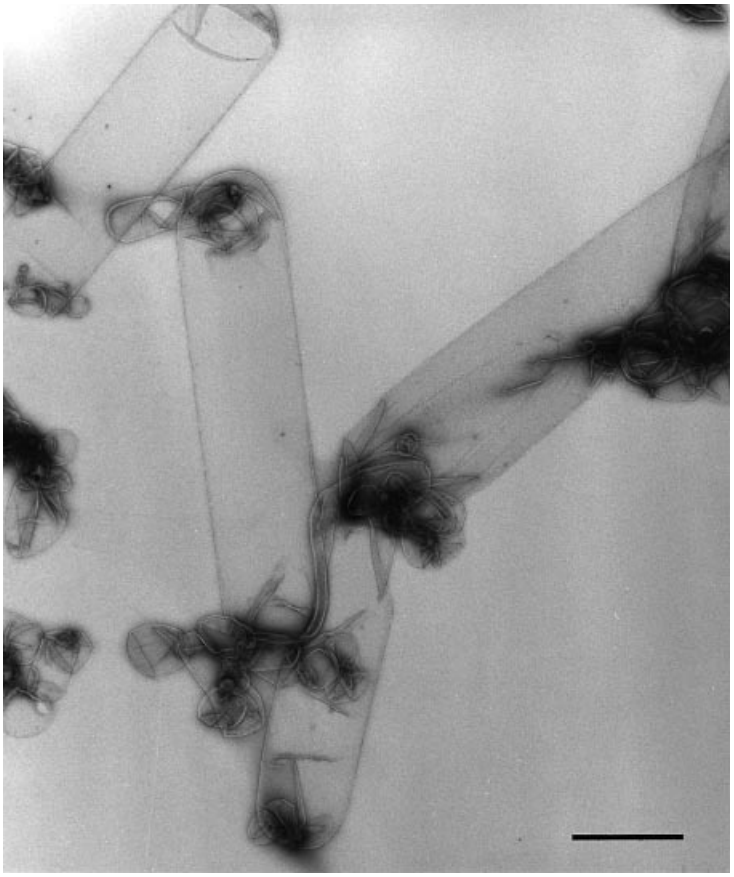

Fig. 1. Electron micrograph of two-dimensional crystals of NhaA (48×181 Å lattice) negatively stained with 2% uranyl acetate. The crystals exhibit a tubular morphology with overall dimensions of (0.4–1.0)×(0.7–4.0) μm or more. Scale bar corresponds to 1.0 μm.

to form two planar lattices which can be processed independently. They are obtained at low pH where NhaA is expected to be in a conformation associated with the inactive state. It is not clear whether the production of well ordered crystals requires that NhaA be held in this inactive state or is due instead to pH-dependent behavior of the crystallization mixture.

Two slightly different crystal forms were obtained under the crystallization regime used in this study depending upon the choice of dialysis buffer. Crystals exhibiting unit cell dimensions of 48×181 Å (hereafter described as the smaller unit cell) were obtained when the dialysis buffer contained a mixture of glycerol and methylpentanediol (MPD), while crystals with a slightly larger unit cell of 48×191 Å (the larger unit cell) were obtained when only glycerol was present in the dialysis buffer. The crystals with the smaller unit cell form the focus of this study as these crystals were more highly ordered, larger, more stable and more reproducible. Low-dose images of frozen-hydrated crystals preserved in tannin show strong reflections at ~8 Å by optical diffraction, and after correction for lattice distortions yield structure factors beyond 4.0 Å resolution (Figure 2A). Images of crystals exhibiting the larger unit cell show reflections at ~13 Å by optical diffraction, and after correction for lattice distortions yield structure factors beyond 8.0 Å resolution. Both crystal forms exhibit $p22_12_1$ symmetry on the basis of phase comparisons of symmetry-related reflections (Valpuesta *et al*., 1994). A projection map of NhaA crystals, with data truncated at 8 Å resolution and with $p22_12_1$ symmetry enforced (Figure 3A) from exhibiting the small unit cell was calculated after merging data from three independent lattices (Table I; Figure 2B), whereas the 8 Å map from exhibiting the large unit cell was calculated from a single image (Figure 3B). In both crystal forms, a unit cell contains four molecules of NhaA which appear as dimers related by a crystallographic 2-fold axis perpendicular to the membrane, and two additional 2-fold screw axes perpendicular to *a* and *b*. This results from the dimers being present in alternately up and down orientations. There is excellent overall agreement within each NhaA molecule between the two maps. However, the packing of dimers is different in the two crystal forms. The dimers in the smaller unit cell are rotated ~20° resulting in closer inter-dimer packing and the introduction of additional close contacts between dimers presumably resulting in better crystalline order. It is not known whether NhaA occurs *in vivo* and is active as a monomer or dimer, so it should be kept in mind that the dimer observed in these projection maps may simply reflect favorable crystallographic interactions.

A dimer of NhaA at 4.0 Å resolution is shown in Figure 3C, with a putative monomer outlined. The molecular boundaries of the dimer were apparent from the large spacing between dimers in crystals exhibiting the large unit cell. NhaA is predicted to have 12 TM helices with relatively short connecting loops (Rothman *et al*., 1996). As a result, the density observed in projection should arise predominantly from these TM helices. NhaA exhibits a relatively open, irregular structure with overall dimensions

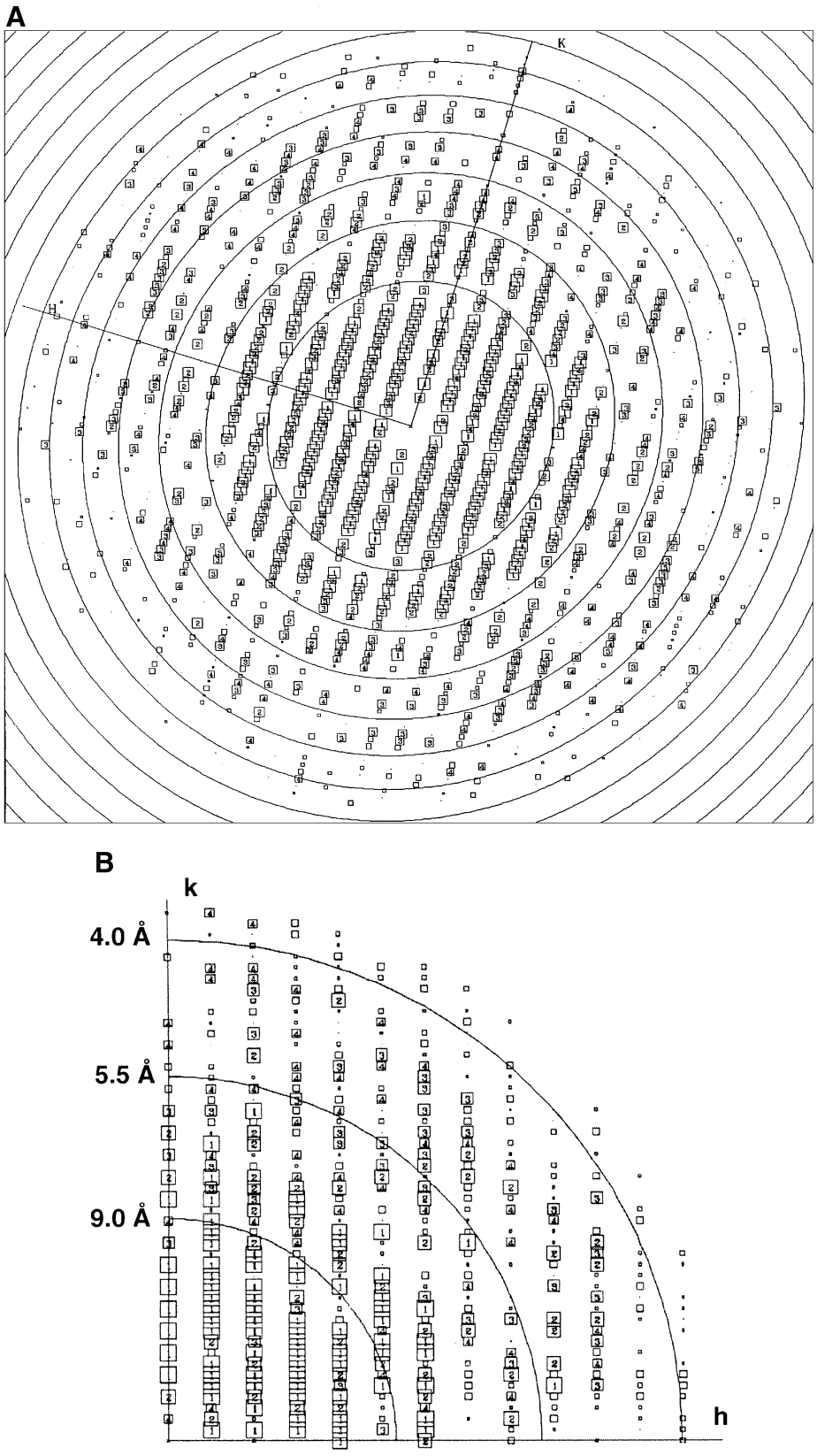

Fig. 2. (**A**) Calculated Fourier transform of an image of a 2D crystal of NhaA exhibiting the 48×181 Å lattice. Each square on the reciprocal lattice describes a Fourier component with the size of the square and number reflecting its signal to noise ratio (Henderson *et al.*, 1986). The largest boxes and smallest numbers describe the most significant reflections. Concentric rings indicate the zero crossings of the contrast transfer function. Fourier components were plotted to 3.5 Å resolution. (**B**) Combined phase error to 3.7 Å resolution for the 48×181 Å lattice after merging three lattices from separate images. The size of the boxes correspond to the phase error after averaging and rounding to 0° or 180° associated for each measurement (1, <8°; 2, <14°; 3, <20°; 4, <30°; 5, <40°; 6, <50°; 7, <70°; 8, <90°, where 90° is random). Values from 1–4 are shown as numbers inside boxes, whereas those from 5–8 are indicated with decreasing box size.

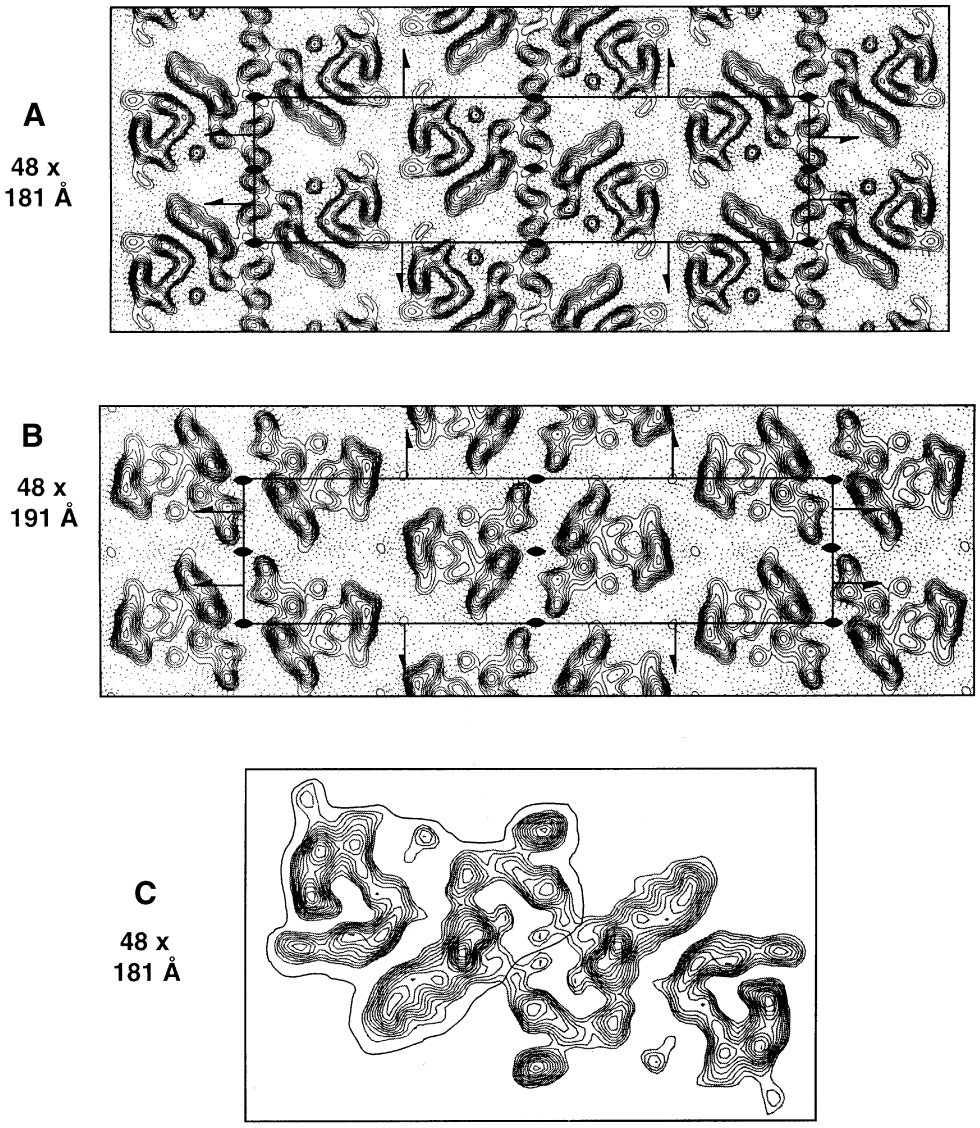

Fig. 3. (**A**) Projection density map of NhaA at 8 Å resolution calculated from merged amplitudes and phases from three independent lattices (48×181 Å) with $p22_12_1$ symmetry enforced. The 2-fold axes perpendicular to the membrane plane and the screw axes parallel to *a* and *b* are shown. A unit cell is displayed with the *a*-axis (48 Å) vertical and the *b*-axis (181 Å) horizontal. One unit cell contains four molecules of NhaA, with two molecules situated in the center of the unit cell. NhaA exhibits a relatively open structure with >10 density peaks visible. Solid lines indicate density above the mean while negative contours are shown as dotted lines. The map was scaled to a maximum density of 250 and contoured in steps of 28 (r.m.s. density = 83.5). The phases were constrained to 0° or 180° since the projection is centrosymmetric. An isotropic temperature factor (B = –200) was applied to compensate for the resolution dependent degradation of image amplitudes (Unger and Schertler, 1995; Unger *et al*., 1997). (**B**) Projection density map of NhaA at 8 Å resolution calculated from amplitudes and phases from a single image of crystals exhibiting the larger unit cell with dimensions 48×191 Å, and with $p22_12_1$ symmetry enforced. The phase errors after rounding to 0° or 180° were 9.3° to 16 Å, 16.5° to 11.3 Å, 23.3° to 9.2 Å and 38.2° to 8 Å with the overall error for 91 reflections to 8 Å being 20.4°. A temperature factor (B = –200) was applied to compensate for the resolution dependent degradation of image amplitudes. The map was scaled to a maximum density of 250 and contoured in steps of 21 (r.m.s. density = 74.0). The two maps exhibit excellent overall agreement. Minor discrepancies between the maps probably reflect differences in phase statistics and completeness, although it is possible that NhaA may exhibit slightly different conformations depending upon the crystal form. (**C**) A dimer of NhaA exhibiting the 48×181 lattice at 4.0 Å resolution with only positive contours shown. A putative monomer is outlined. A temperature factor of B = –50 was used to compensate partially for the resolution-dependent degradation of image amplitudes. The map was scaled to a maximum density of 250 and contoured in steps of 17.2 (r.m.s. density = 68.9).

of ~38×48 Å which is consistent with a 42 kDa bundle of TM helices. Perhaps the most striking feature of the map is the marked asymmetry evident within NhaA in projection. There is a ring- or 'C'-shaped density feature adjacent to an elongated region of density which exhibits a number of peaks including several which are relatively distant from the remainder of the molecule. The ring-shaped feature is not well resolved into individual peaks, possibly indicative of a bundle of tilted TM helices. There are several particularly strong density peaks which may correspond to TM helices oriented perpendicular, or nearly so, with respect to the membrane plane. These include a well resolved peak at the end of the elongated region which appears to mediate inter-dimer contacts, as well as a peak in the center of the elongated region and another on the most distant side of the ring-shaped density region. The dimer interface appears to have two principal sites of interaction between monomers.

Table I. Electron crystallographic image statistics

Plane group symmetry[a]	$p22_12_1$
Unit cell dimensions	a = 47.5 ± 0.2 Å b = 181.4 ± 1.2 Å γ = 90°
Number of images and lattices	3
Range of defocus	3440–7330 Å
Total number of observations[b]	1080
Number of unique observations[b]	426
Overall phase residual to 4.0 Å[c]	19.9°

Resolution range (Å)	Number of unique reflections	Phase residual[c] (random = 45°)
200.0–9.1	83	8.6
9.1–6.4	78	16.0
6.4–5.2	76	23.9
5.2–4.5	70	22.7
4.5–4.1	64	28.9
4.1–3.7	55	34.5

[a]Symmetry was determined using ALLSPACE (Valpuesta *et al*., 1994). For example, for lattice 4572 the phase residual for plane group $p22_12_1$ to 4 Å resolution was 37.1° (1263 comparisons of reflections with IQ ⩽7), in good agreement with the target residual 38.0°. For the same lattice, the phase residual for $p22_12_1$ to 6 Å resolution was 26.6° (769 comparisons), compared with the target residual of 27.3°. As expected, plane groups of lower symmetry with 2-fold symmetry and screw axes (*p*2, *p*121b and *p*121a), were either as good as or close to their target residuals, however, with considerably fewer phase comparisons than $p22_12_1$.
[b]Including reflections with IQ ⩽7 to 3.7 Å.
[c]Amplitude weighted, vectorially averaged phase residual which shows the phase deviation from theoretical 0°/180° (45° is random). The overall phase error associated with merging the three images to 4 Å resolution, without the deviation from 0°/180°, was 25.2° (90° is random).

Many 12 TM secondary transporters are postulated to have arisen from the duplication of an ancient six TM segment. However, sequence analysis of NhaA does not give evidence for internal duplication. The 12 TM secondary transporter motif is perhaps the most commonly predicted topology, but it is not clear whether these proteins will form a homogeneous group with respect to structure. Clearly, not all 12 TM proteins have the same structure as is shown, for example, by subunit I of cytochrome *c* oxidase which displays apparent 3-fold symmetry with helices organized into three 4-helix bundles (Iwata *et al*., 1995), which is clearly different from the TM helix organization found in NhaA. Proteins which function as channels and facilitate bi-directional substrate flow across membranes frequently exhibit a high degree of symmetry. For example, oligomeric channel proteins such as the *Streptomyces lividans* K^+ channel displays 4-fold symmetry (Doyle *et al*., 1998), while the gap junction exhibits 6-fold symmetry (Unger *et al*., 1997). The monomeric channel protein AQP1 displays apparent local near-2-fold symmetry in the three-dimensional structure (Cheng *et al*., 1997; Li *et al*., 1997; Walz *et al*., 1997). In contrast, transport proteins which exhibit directionality in their transport reactions, such as the H^+-ATPase (Auer *et al*., 1998), Ca^{2+}-ATPase (Zhang *et al*., 1998), bacteriorhodopsin (Henderson *et al*., 1990) and NhaA, do not exhibit such symmetry in projection.

The ring-shaped feature of NhaA is reminiscent of the AQP1 projection structure (Mitra *et al*., 1995; Walz *et al*., 1995), which has been shown to consist of a bundle of six highly tilted TM helices (Cheng *et al*., 1997; Li *et al*., 1997; Walz *et al*., 1997). The dimensions differ, however, with the AQP1 helix bundle exhibiting a diameter of ~32 Å, whereas in NhaA the ring-like structure is smaller, ~23 Å in diameter. The projection map of NhaA also bears some resemblance to the organization of TM helices in the H^+-ATPase (Auer *et al*., 1998). The H^+-ATPase has 10 TM helices which are organized into a right-handed four-helix bundle. This is covered on one side by a layer of four helices which are, in turn, covered by a further layer of two helices. A similar arrangement could be envisioned in NhaA based on the projection maps in Figure 3.

The exact number of TM helices, their relative orientations and assignment in the protein sequence cannot be resolved from the projection structure of NhaA. This will require the calculation of a three-dimensional map, which is currently under way.

Materials and methods

Overexpression and purification

NhaA was overexpressed with a C-terminal His_6 tag in *E.coli* BL21(DE3) from a PET construct (Olami *et al*., 1997), grown overnight at 30°C in 2× TY medium (1.6% tryptone, 2% yeast extract, 86 mM NaCl) plus ampicillin. Overexpression occurred without IPTG induction by exploiting the leaky T7 promoter, and in spite of the presence of an endogenous NhaA background present in BL21(DE3). Total *E.coli* membranes were isolated from cells disrupted by passing several times through a microfluidizer, harvested by differential centrifugation and stored at 10 mg/ml protein at –20°C. Membranes were solubilized in 1% dodecyl β-D-maltoside (DDM) for 20 min at 23°C and were then bound to Ni^{2+}-NTA resin (Qiagen) in a batch at 23°C for 15 min or 1 h at 4°C, transferred to a column and washed with 30 mM imidazole (pH 8.0) and 300 mM NaCl. NhaA was then eluted with 25 mM K^+ acetate pH 4, 300 mM KCl, 30% glycerol and 0.1–0.02% DDM, and stored at 4°C.

Two-dimensional crystallization

Crystallization was performed by dialysis of a solution containing ~0.8 mg/ml protein and *E.coli* polar lipids (Avanti Polar Lipids) at lipid to protein ratios of 0.2–0.5 (w/w). Dialysis of 50–100 μl samples was performed in glass capillaries (Kühlbrandt, 1992) or Dispo-biodialyzers (AmiKa Corp.) and 300–500 μl samples in Slide-a-lysers (Pierce). Dialysis against 25 mM K^+ acetate pH 4, 150 mM KCl, 0.1 mM $GdCl_3$, 5% glycerol, 5% MPD and 3 mM NaN_3 resulted in well-ordered crystals exhibiting a unit cell of ~48×181 Å after 4–6 days at 37°C which were stable upon storage at 4°C for several weeks. Dialysis against the same buffer except with no MPD and in the presence of 10% glycerol produced crystals exhibiting a unit cell of 48×191 Å.

Electron microscopy

Negatively stained grids were prepared with 2% uranyl acetate, and images recorded using a Philips CM12 or CM120 microscope at a magnification of 45 000×. Frozen-hydrated specimens were prepared by the back injection of a 2 μl aliquot of the crystal solution into a 0.6% tannin pH 6 solution on continuous carbon film on a copper or molybdenum grid, blotted and rapidly frozen in liquid N_2 (Wang and Kühlbrandt, 1991). Images were recorded using a JEOL 3000 SFF equipped with a field emission gun and liquid helium cooled top entry stage using a 0° tilt holder, with an accelerating voltage of 300 kV at a nominal specimen temperature of 4 K and a magnification of 53 300× or 70 000×. Images were either recorded in flood beam mode with a 1 s exposure time at an estimated electron dose of 20–30 electrons/$Å^2$, or using a spot scan procedure with an exposure time of 40 ms per spot and a similar total dose. Images were recorded on Kodak SO-163 electron emulsion film and developed for 12 min in full-strength Kodak D19 developer. Images were evaluated by optical diffraction and those exhibiting strong reflections at ~8–13 Å resolution were selected for further analysis.

Image processing

Well ordered areas of 6000×6000 pixels corresponding to ~4 cm on the negatives were digitized using a 7 μm pixel size on a Zeiss SCAI scanner. Images were processed using MRC image processing programs to correct for lattice distortions, the contrast transfer function, astigmatism and beam tilt (Henderson *et al*., 1986; Crowther *et al*., 1996). Comparison of phase residuals (Valpuesta *et al*., 1994) revealed $p22_12_1$ symmetry.

Acknowledgements

K.A.W. is especially grateful to Deryck Mills for assistance with microscopy and Manfred Auer for assistance with image processing. K.A.W. thanks Vinzenz Unger and Janet Vonck for advice on image processing, Michael Way for advice on protein expression and purification, and Andrea Rothman for her assistance with NhaA biochemistry in the early stages of this project. This work has been partially funded by the BMBF and supported by BMBF's international bureau at the DLR (Deutsch-Israelisches Projekt). This work was supported by a long term fellowship to K.A.W. from the Human Frontiers Science Program.

References

Auer,M., Scarborough,G. and Kühlbrandt,W. (1998) Three-dimensional map of the plasma membrane H^+-ATPase in the open conformation. *Nature*, **392**, 840–843.

Cheng,A., van Hoek,A.N., Yeager,M., Verkman,A.S. and Mitra,A. (1997) Three-dimensional organization of a human water channel. *Nature*, **387**, 627–630.

Crowther,R.A., Henderson,R. and Smith,J.M. (1996) MRC image processing programs. *J. Struct. Biol.*, **116**, 9–16.

Dolder,M., Walz,T., Hefti,A. and Engel,A. (1993) Human erythrocyte band 3. Solubilization and reconstitution into two-dimensional crystals. *J. Mol. Biol*., **231**, 119–132.

Doyle,D.A., Cabral,J.M., Pfuetzner,R.A., Kuo,A., Gulbis,J.M., Cohen,S.L., Chait,B.T. and MacKinnon,R. (1998) The structure of the potassium channel: molecular basis of K^+ conduction and selectivity. *Science*, **280**, 69–77.

Henderson,R., Baldwin,J.M., Downing,K.H., Lepault,J. and Zemlin,F. (1986) Structure of purple membrane from *Halobacterium halobium*: recording, measurement and evaluation of electron micrographs at 3.5 Å resolution. *Ultramicroscopy*, **19**, 147–178.

Henderson,R., Baldwin,J.M., Ceska,T.A., Zemlin,F., Beckmann,E. and Downing,K.H. (1990) Model for the structure of bacteriorhodopsin based on high-resolution electron cryo-microscopy. *J. Mol. Biol*., **213**, 899–929.

Iwata,S., Ostermeier,C., Ludwig,B. and Michel,H. (1995) Structure at 2.8 Å resolution of cytochrome *c* oxidase from *Paracoccus denitrificans*. *Nature*, **376**, 660–669.

Kimura,Y. *et al*. (1997) Surface of bacteriorhodopsin revealed by high-resolution electron crystallography. *Nature*, **389**, 206–211.

Kühlbrandt,W. (1992) Two-dimensional crystallization of membrane proteins. *Quart. Rev. Biophys.*, **25**, 1–49.

Kühlbrandt,W., Wang,D.N. and Fujiyoshi,Y. (1994) Atomic model of plant light-harvesting complex by electron crystallography. *Nature*, **367**, 614–621.

Li,H., Lee,S. and Jap,B. (1997) Molecular design of aquaporin-1 water channel as revealed by electron crystallography. *Nature Struct. Biol*., **4**, 263–265.

Mitra,A.K., van Hoek,A.N., Wiener,M.C., Verkman,A.S. and Yeager,M. (1995) The CHIP28 water channel visualized in ice by electron crystallography. *Nature Struct. Biol*., **2**, 726–729.

Olami,Y., Rimon,A., Gerchman,Y., Rothman,A. and Padan,E. (1997) Histidine 225, a residue of the NhaA-Na^+/H^+ antiporter of *Escherichia coli* is exposed and faces the cell exterior. *J. Biol. Chem*., **272**, 1761–1768.

Padan,E. and Schuldiner,S. (1994a) Molecular physiology of Na^+/H^+ antiporters, key transporters in circulation of Na^+ and H^+ in cells. *Biochim. Biophys. Acta*, **1185**, 129–151.

Padan,E. and Schuldiner,S. (1994b) Molecular physiology of the Na^+/H^+ antiporter in *Escherichia coli*. *J. Exp. Biol*., **196**, 443–456.

Padan,E. and Schuldiner,S. (1996) Bacterial Na^+/H^+ antiporters—molecular biology, biochemistry and physiology. In Konings,W.N., Kaback,H.R. and Lolkema,J.S. (eds), *Handbook of Biological Physics*. Vol. 2. Elsevier Science, Oxford, UK pp. 501–531.

Paulsen,I.T., Sliwinski,M.L. and Saier,M.H. (1998) Microbial genome analyses: global comparisons of transport capabilities based on phylogenies bioenergetics and substrate specificities. *J. Mol. Biol*., **277**, 573–592.

Rigaud,J.-L., Mosser,G., Lacapere,J.-J., Olofsson,A., Levy,D. and Ranck,J.-L. (1997) Bio-beads: an efficient strategy for two-dimensional crystallization of membrane proteins. *J. Struct. Biol.*, **118**, 226–235.

Rothman,A., Padan,E. and Schuldiner,S. (1996) Topological analysis of NhaA, a Na^+/H^+ antiporter from *Escherichia coli*. *J. Biol. Chem*., **271**, 32288–32292.

Rothman,A., Gerchman,Y., Padan,E. and Schuldiner,S. (1997) Probing the conformation of NhaA, a Na^+/H^+ antiporter from *Escherichia coli*, with trypsin. *Biochemistry*, **36**, 14572–14576.

Taglicht,D., Padan,E. and Schuldiner,S. (1991) Overproduction and purification of a functional Na^+/H^+ antiporter coded by nhaA (ant) from *Escherichia coli*. *J. Biol. Chem.*, **266**, 11289–11294.

Unger,V.M. and Schertler,G.F.X. (1995) Low resolution structure of bovine rhodopsin determined by electron cryo-microscopy. *Biophys. J.*, **68**, 1776–1786.

Unger,V.M., Kumar,N.M., Gilula,N.B. and Yeager,M. (1997) Projection structure of a gap junction membrane channel at 7 Å resolution. *Nature Struct. Biol.*, **4**, 39–43.

Valpuesta,J.M., Carrascosa,J.L. and Henderson R. (1994) Analysis of electron microscope images and electron diffraction patterns of thin crystals of Ø29 connectors in ice. *J. Mol. Biol.*, **240**, 281–287.

Walz,T. and Grigorieff,N. (1998) Electron crystallography of two-dimensional crystals of membrane proteins. *J. Struct. Biol*., **121**, 142–161.

Walz,T., Typke,D., Smith,B.L., Agre,P. and Engel,A. (1995) Projection map of aquaporin-1 determined by electron crystallography. *Nature Struct. Biol*., **2**, 730–732.

Walz,T. *et al*. (1997) The three-dimensional structure of aquaporin-1. *Nature*, **387**, 624–627.

Wang,D.N. and Kühlbrandt,W. (1991) High-resolution electron crystallography of light-harvesting chlorophyll *a/b*-protein complex in three different media. *J. Mol. Biol*., **217**, 691–699.

Wang,D.N., Kühlbrandt,W., Sarabia,V.E. and Reithmeier,R.A.F. (1993) Two-dimensional structure of the membrane domain of human band 3, the anion transport protein of the erythrocyte membrane. *EMBO J*., **12**, 2233–2239.

Wang,D.N., Sarabia,V.E., Reithmeier,R.A.F. and Kühlbrandt,W. (1994) Two-dimensional structure of the membrane domain of human Band 3, the anion transport protein of the erythrocyte membrane. *EMBO J*., **13**, 3230–3235.

Zhang,P., Toyoshima,C., Yonekura K., Green,N.M. and Stokes,D.L. (1998) Structure of the calcium pump from sarcoplasmic reticulum at 8 Å resolution. *Nature*, **392**, 835–839.

Zhuang,J., Privé,G.G., Werner,G.E., Ringler,P., Kaback,H.R. and Engel,A. (1999) Two-dimensional crystallization of Escherichia coli lactose permease. *J. Struct. Biol*., **125**, 63–75.

Received March 8, 1999; revised and accepted May 18, 1999